Available online at www.sciencedirect.com

ScienceDirect

Transportation Research Procedia 91 (2025) 624–631

Transportation Research Procedia

www.elsevier.com/locate/procedia

The Science and Development of Transport - TRANSCODE 2025

Optimization of Geometry and Material Properties in Jointed Plain Concrete Pavement (JPCP)

Ali Pirdavani[a,b,*], Tinne Bollen[a], Senne Ools[a], Stigg Verheyen[a]

[a]*UHasselt, Faculty of Engineering Technology, Agoralaan, Diepenbeek 3590, Belgium*
[b]*UHasselt, The Transportation Research Institute, Martelarenlaan 42, Hasselt 3500, Belgium*

Abstract

This study evaluates the influence of slab geometry and subbase type on the fatigue performance of jointed concrete pavements, using allowable load repetitions as the primary performance indicator. Four design scenarios featuring different slab widths, lengths, and subbase materials were analyzed using EverFE finite element modeling and the PCA fatigue criteria. The results demonstrate that pavements with a stabilized crushed stone subbase consistently achieve higher allowable repetitions compared to those with a lean concrete subbase. Furthermore, configurations with three slabs outperform two-slab setups regarding fatigue resistance. Optimal performance within each scenario is associated with a low length-to-thickness ratio, which in this study was limited to a minimum value of 25, and a length-to-width ratio close to 1.14. The highest fatigue performance overall was observed for a length-to-width ratio of 1.24 combined with the lowest length-to-thickness ratio tested. These findings highlight the significant impact of slab configuration and subbase selection on pavement fatigue life, providing valuable guidance for early-stage pavement design to enhance durability.

Keywords: Jointed Plain Concrete Pavement (JPCP); EverFE; Slab geometry; Subbase type; Fatigue performance; Allowable load repetitions

1. Introduction

Concrete pavements have long been a fundamental element in road infrastructure due to their durability, structural capacity, and relatively low maintenance requirements. Despite the many advantages of concrete pavements, cracking

* Corresponding author. Tel.: +32 11 29 2183
E-mail address: ali.pirdavani@uhasselt.be

10.1016/j.trpro.2025.10.080

is quite a common problem. Yet, no single factor can be designated as the primary cause of transverse cracking. Cracking is a combination of multiple factors, such as curling of the concrete slab due to temperature gradients, fatigue due to repeated traffic loads, and the improper control of the shrinkage of the concrete in the early stages of construction, as stated in Chen et al. (2002). Jointed Plain Concrete Pavement (JPCP) relies on strategically placed joints to control cracking and intentionally locate cracks at these joints, as stated by Rens (2020). In this way, the cracks' location and width are managed.

The primary objective of this study is to optimize the design of JPCP in order to minimize fatigue cracking and thereby improve the long-term performance and sustainability of concrete pavements. The research question this study will answer is: What are the optimal dimensions and layer composition of JPCP to maximize performance in terms of allowable load repetitions?

The finite element analysis tool EverFE was employed to compare the pavement performance. This study evaluates pavement performance only based on the Portland Cement Association (PCA) methodology for fatigue cracking.

2. Method and materials

2.1. Software

The software package EverFE was used for this study, designed by researchers from the Universities of Maine and Washington (2025) in the United States. This 3D finite-element analysis tool simulates the responses of JPCP.

2.2. Scenarios

Four main scenarios were developed for the pavement design of a regional road with two lanes and a breakdown lane. The regional road consists of three layers: concrete slabs, a base layer, and a variable subbase layer. Scenario 1 considers three rows of concrete slabs and is then subdivided into scenarios 1.1 and 1.2, which differ based on the subbase layer. Scenario 1.1 uses stabilized crushed stone as the subbase layer, and scenario 1.2 uses lean concrete. Scenario 2 then assumes two wider rows of concrete slabs and is divided into scenarios 2.1 and 2.2, which differ in the same way as scenario 1. An overview of the four main scenarios is shown below in Fig. 1.

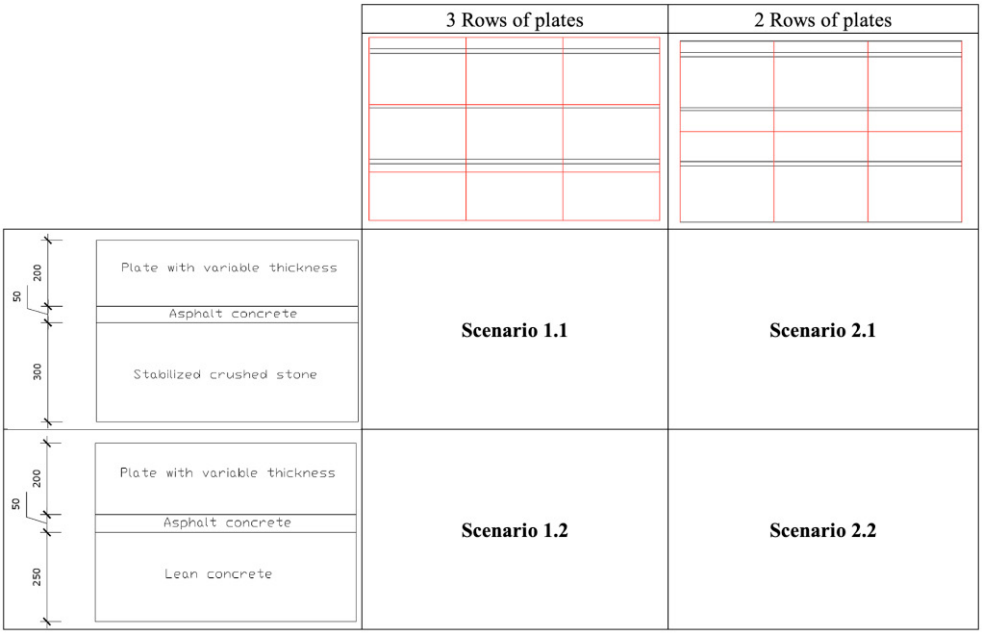

Fig. 1. Overview of research scenarios.

Each scenario has been worked out for different lengths and thicknesses of the concrete slab. According to the Guide for Design of Jointed Plain Concrete Pavements authored by Rens (2020), the length of the concrete slabs is limited by three factors as follows:

- Length over width (L/w) ≤ 1.50
- L ≤ 25×T
- 5.00 m ≤ L ≤ 7.00 m

The first rule states that the shape of the slab should be as square as possible. In the case of long, narrow slabs, the slab starts to behave like a beam and thus increases the risk of curling or excessive bending, which increases bending tensile stresses. The second rule establishes a relationship between the length and thickness of the slab. A factor of 25 can be considered safe. For the development of the scenarios in this study, assumptions outside the framework of the established guidelines were adopted. This approach aimed to examine the impact of these assumptions on the behavior of the concrete slabs, specifically concerning the development of tensile stresses.

The length of the concrete slabs across all scenarios ranges from 4,500 mm to 9,000 mm, with various thicknesses examined for each length. The length and thickness combinations considered are summarized in Table 1. In scenarios 1.1 and 1.2, the slabs in the first and second rows have a width of 4,450 mm, while those in the third row have a width of 3,200 mm. In scenarios 2.1 and 2.2, the slab width in the first and second rows is 6,050 mm. In total, 104 scenarios are analyzed in this study.

Table 1. Overview of considered lengths and thicknesses: Scenarios 1.1, 1.2, 2.1, and 2.2.

Scenario	Length (mm)	Thicknesses (mm)			
1.1 & 1.2	4,500	120	140	160	180
	5,000	140	160	180	200
	5,500	160	180	200	220
	6,000	180	200	220	240
	6,500	200	220	240	260
	7,000	220	240	260	280
2.1 & 2.2	6,100	185	205	225	245
	6,500	200	220	240	260
	7,000	220	240	260	280
	7,500	240	260	280	300
	8,000	260	280	300	320
	8,500	280	300	320	340
	9,000	300	320	340	360

2.3. Parameters

In this study, several key parameters were identified and analyzed to evaluate the performance of JPCP. These parameters include material parameters, which encompass the mechanical properties of the concrete and subbase materials; loading parameters, which account for traffic loads and their impact on pavement behavior; dowel parameters, which relate to the design and configuration of the dowels used for load transfers between slabs; and interlock parameters, which influence the load transfer between adjacent slabs. The specific values used for these parameters were derived from a thorough review of relevant literature.

2.3.1. Material Parameters

In this study, the properties of the concrete slabs, dowels, and tie bars are assumed to be constant across all scenarios to maintain consistency in the analysis. In contrast, variations are introduced in the base and subbase layers to evaluate their influence on pavement performance. Specifically, two types of subbase materials are considered: stabilized crushed stone and lean concrete, both combined with an asphalt concrete base. These differences are designed to reflect realistic construction practices and to investigate the impact of foundation properties on the response of the pavement under traffic and environmental loads. An overview of all material parameters used in the analysis is provided in Table 2.

Table 2. Material parameters.

Material	Parameter	Value
Concrete slab	E (MPa)	27,000 from Matrix Software (2023)
	ν (-)	0.15 from Gu et al. (2019)
	α (1/ºC)	10E-6 from Lingannagari et al. (2003)
	ρ (kg/m^3)	2,300 from Nawy (2008)
Dowels and Ties	E (MPa)	200,000 from Gu et al. (2019)
	ν (–)	0.3 from Gu et al. (2019)
Asphalt Concrete (Base)	E (MPa)	2,750 (20ºC) from Xu (2016)
	ν (–)	0.2 (20ºC) from Xu (2016)
	ρ (kg/m^3)	2,300 from Engineering Tips (2004)
Stabilized crushed stone (Subbase)	E (MPa)	15,000 from Skar (2017)
	ν (–)	0.2 (20ºC) from Skar (2017)
	ρ (kg/m^3)	1,580 from Majer et al.(2024)
Lean concrete (Subbase)	E (MPa)	10,000 from Lijun and Xinwu (2012)
	ν (–)	0.15 from Lijun and Xinwu (2012)
	ρ (kg/m^3)	2,250 from Ecoinvent (2013)

2.3.2. Loading Parameters

The loading parameters in this study simulate a dual-wheel tandem axle with a wheel load of 100 kN, representing realistic heavy vehicle traffic and replicating pavement response under typical service conditions.

The geometry is defined by five parameters: tire contact length L = 200 mm, width W = 150 mm, transverse spacing B = 300 mm, center-to-center spacing A = 1,500 mm, and longitudinal axle spacing S = 1,800 mm.

Load placement significantly affects stress and deflection in JPCP. Edge loading produces high localized stresses, contributing to fatigue cracking. Therefore, the load is applied near the longitudinal edge, midway between two transverse joints, the most critical position for inducing fatigue damage as specified by Yan and Wei (2023).

For this case, the load is positioned at the longitudinal midpoint of the slab and placed as close as practically possible to the edge. Due to the presence of lane markings, the load cannot be placed directly at the edge. Instead, it is applied adjacent to the marking, corresponding to a realistic wheel path while preserving critical loading conditions. The load placement for scenarios 1 and 2 is illustrated in Fig. 2.

In addition to mechanical loading, a temperature gradient was applied to simulate environmental effects on the slab behavior. A linear temperature profile was imposed, with a temperature of 20ºC at the top and 0ºC at the bottom surface of the slab. This thermal loading induces upward slab curling, introducing additional stresses that interact with those generated by mechanical loading.

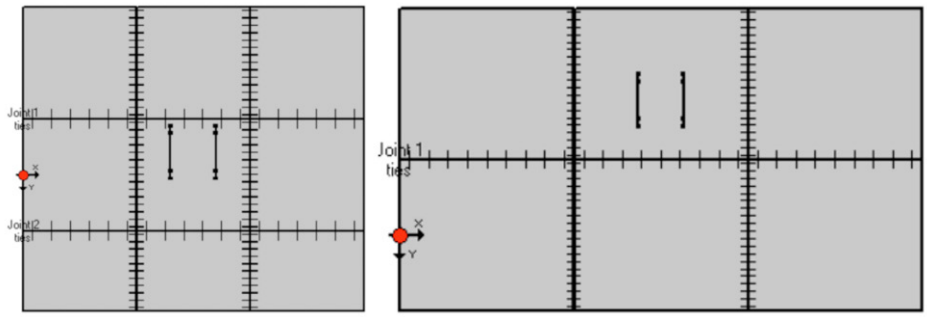

Fig. 2. Load placement for Scenario 1 (left) and Scenario 2 (right).

2.3.3. Dowel and Ties Parameters

The dowel parameters in this study represent the load transfer elements installed across transverse joints to enhance the structural continuity of JPCP. A standardized dowel bar configuration is adopted across all scenarios to ensure consistency throughout the analysis.

The diameter of the dowel bars is defined as 30 mm, with an embedment length of 300 mm into the adjacent concrete slab. The distance from the outermost dowel to the slab edge is consistently applied as 150 mm, defined by Agentschap Wegen en Verkeer – Vlaamse Overheid (2019).

Tie bars are implemented across longitudinal joints to provide longitudinal restraint and maintain slab alignment. This study modeled tie bars with a diameter of 16 mm and an embedment length of 400 mm into the adjacent concrete slab (Gu et al., 2019). To prevent interference with dowel bars, the spacing of the tie bars is adjusted for each slab length, ensuring no overlap occurs between the two types of reinforcement.

The dowel-slab and tie-slab support moduli are both 1,000 MPa. These values represent the local stiffness of the concrete surrounding the dowels and tie bars and directly influence their effectiveness in transferring loads across the joints. The dowel-slab restraint modulus is defined as 0 MPa to reflect the function of the dowels, which are intended to allow free longitudinal movement and thus avoid restraint forces at the joints. In contrast, the tie-slab restraint modulus is set at 10,000 MPa, capturing the substantial longitudinal restraint provided by tie bars. This restraint is crucial for limiting joint opening and maintaining slab continuity, as declared by Shaban et al. (2020).

The number of dowels installed across the joints varies depending on the scenario analyzed. In scenario 1, fifteen dowels are positioned in the first and second rows, while eleven are placed in the third row. For scenario 2, the first and second rows have twenty dowels each. The number of dowels per slab was selected to achieve an approximate spacing of 300 mm between adjacent dowels. The reduced number of dowels in scenario 1 is attributed to the narrower slab width compared to scenario 2.

2.3.4. Interlock Parameters

The interlock behavior at the joints is modeled using a linear approach, simplifying the simulation while capturing the essential response. An opening between columns of 0.5 mm is defined, representing the allowable relative movement before the aggregate interlock becomes active. The joint stiffness is set to 0 MPa/mm, assuming that no additional stiffness is provided once the joint opens, thereby focusing the load transfer primarily through the dowel bars and tie bars.

2.4. Testing method

The finite element analysis tool EverFE is employed to compare the pavement performance across the four scenarios. This study evaluates pavement performance only based on the PCA methodology for fatigue cracking. According to the AASHTO Guide for Design of Pavement Structures (1993), the ratio between allowable and expected load repetitions is a key parameter in performance assessment, further certified by Swarna et al. (2024). Following the PCA method, the most critical stress for fatigue cracking is measured when the load is placed on the slab's edge, as

confirmed by Seric et al. (2013). The bending of the slab under loading conditions results in maximum tensile stresses concentrated at the bottom of the slab, as stated by Agoes and Candra (2021).

The EverFE analysis provides the maximal tensile flexural stress at the most critical location at the bottom of the slab. To calculate the modulus of rupture with formula (1), a characteristic compressive strength of 50 MPa is assumed, defined by Agentschap Wegen en Verkeer – Vlaamse Overheid (2019). The stress ratio (SR) is defined as the ratio between the maximum flexural tensile stress and the modulus of rupture of concrete (i.e., f_{cr}) dependent on the compressive strength of concrete (f_{ck}). This ratio is used to calculate the allowable load repetitions (N) using equations (2), (3), and (4), dependent on different levels of SR, as prescribed by Swarna et al. (2024).

$$f_{cr} = 0.7 \cdot \sqrt{f_{ck}} \tag{1}$$

$$N = \infty \qquad for\ SR < 0.45 \tag{2}$$

$$N = \left[\frac{4.2577}{SR - 0.4325}\right]^{3.268} \qquad for\ 0.45 \leq SR \leq 0.55 \tag{3}$$

$$log\ N = \frac{0.9718 - SR}{0.0828} \qquad for\ SR \geq 0.55 \tag{4}$$

3. Results and discussion

The results consist of the allowable repetitions calculated for each thickness-length combination specified across the four different scenarios. The length-to-thickness ratio and length-to-width ratio are used to compare the different situations.

3.1. Allowable repetitions

Fig. 3 shows the results for the calculated allowable repetitions as a function of the length-to-thickness ratio for each scenario, categorized by a specific length-to-width ratio, and is used to compare the order of magnitude of the allowable repetitions. The allowable repetitions are calculated solely based on the occurrence of fatigue cracking. Fig. 3 shows an overall negative trend between the allowable repetitions and the length-to-thickness ratio. This indicates that increasing the slab length while maintaining a constant thickness or decreasing the slab thickness while keeping the length constant reduces performance regarding allowable repetitions.

A comparison of the two subbases indicates that the stabilized crushed stone base, used in scenarios 1.1 and 2.1, demonstrates a significantly better performance than the lean concrete subbases. Considering the optimal geometrical conditions, scenario 1.1 achieves 9,400,000 allowable repetitions, whereas scenario 1.2 reaches only 417,000. Scenario 2.1 sustains up to 407,000 allowable repetitions for the two-plate setup, while scenario 2.2 is limited to 145,000.

A third notable result relates to the performance of the two different plate setups. The three-plate setup in scenario 1 performs significantly better than the two-plate setup in scenario 2. Considering the optimal length and thickness of the plates, scenario 1.1 can reach 9,000,000 more allowable repetitions than scenario 2.1. Scenario 1.2 achieves over 250,000 more allowable repetitions than scenario 2.2. Modifying the plate setup from a three-plate setup to a two-plate setup has a less significant impact when using a lean concrete subbase than when using a stabilized crushed stone subbase.

The optimal ratios, geometrical properties, and performance results, based on the number of allowable repetitions, are shown in Table 3. These values indicate that the best performance is achieved with a length-to-thickness ratio of 25. As this is the lowest tested ratio, it can be concluded that optimal performance is associated with a shorter plate length and a higher plate thickness. In scenario 1.2, the best performance is achieved with a length-to-thickness ratio of 27.5, as also observed in Fig. 3. When considering a three-plate setup, the lean concrete subbase pavement achieves its best performance with a lower length-to-width ratio compared to the stabilized crushed stone subbase, as opposed to the two-plate setup, where the lean concrete subbase requires a higher length-to-width ratio.

Table 3. Optimal results in terms of allowable repetitions for each scenario.

Scenario	Length (mm)	Thickness (mm)	Length over thickness (L/T)	Length over width (L/w)	Allowable Load Repetitions	Stress Ratio
1.1	5,500	220	25	1.24	9.40E6	0.46
1.2	5,000	200	27.5	1.12	4.17E5	0.51
2.1	6,500	260	25	1.07	4.07E5	0.51
2.2	7,000	280	25	1.16	1.45E5	0.54

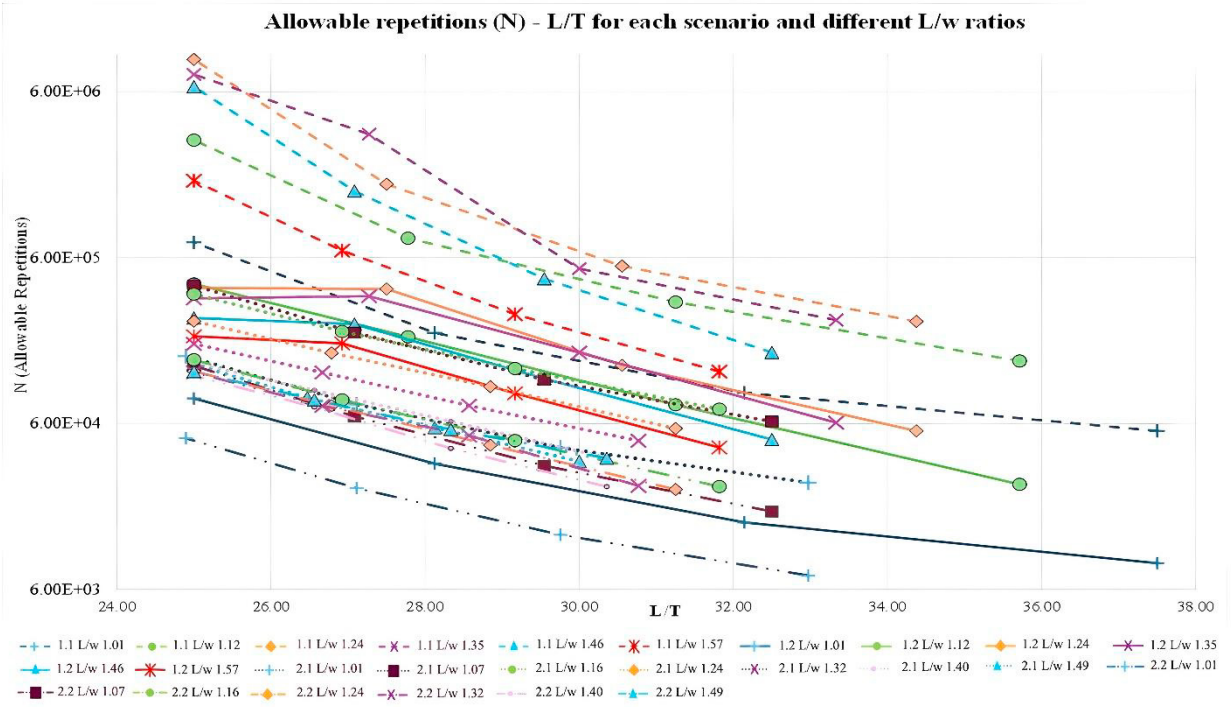

Fig.3. Allowable load repetitions (N) – based on L/T for each scenario and different L/w ratios.

4. Conclusion

Based on a comprehensive evaluation of allowable repetitions, this study identifies the most favorable pavement configuration among the alternatives considered. Pavements incorporating a stabilized crushed stone subbase consistently outperform those constructed with a lean concrete subbase. Additionally, configurations employing a three-plate setup demonstrate higher fatigue resistance compared to two-plate setups. The slab configuration itself appears to have a more pronounced impact on fatigue performance than the choice of subbase material. Therefore, from the perspective of allowable repetitions, the configuration used in scenario 1.1—featuring a three-slab layout combined with a stabilized crushed stone subbase—emerges as the most advantageous design.

Within each scenario, optimal performance is achieved using configurations with a low length-to-thickness ratio, which in this study was limited to a minimum value of 25. Furthermore, the length-to-width ratio also influences fatigue performance: for three-plate setups, a low value of around 1.14 is the most effective, while for two-plate setups, different aspect ratios were explored. The best overall result was obtained with a length-to-width ratio of 1.24, combined with the lowest tested length-to-thickness ratio.

Although lean concrete subbases can still perform adequately under repeated loading, they generally require thicker slabs to compensate for the lower fatigue performance compared to stabilized crushed stone subbases. In contrast, the

stabilized crushed stone subbase achieves high allowable repetitions even at lower thicknesses, making it more favorable when fatigue life is the primary concern.

Overall, the study concludes that a three-slab configuration on a stabilized crushed stone subbase provides the most balanced and effective pavement structure in terms of allowable load repetitions. The results clearly indicate the advantage of combining narrow slab geometry with an optimized subbase material to enhance fatigue resistance. Future research is encouraged to examine the behavior of configurations with length-to-thickness ratios below 25 to determine if further improvements in fatigue performance are feasible.

These insights can help guide early-stage pavement design by illustrating slab geometry's and subbase types' significant influence on fatigue life. Designers can apply this knowledge to achieve more durable, efficient configurations tailored to local conditions and performance expectations.

References

Agoes, S., & Candra, A. (2021). Analysis of the effect of slab thickness on crack width in rigid pavement slabs. *EUREKA: Physics and Engineering, 2021*(2), 42–51.

American Association of State Highway and Transportation Officials. (1993). Guide for design of pavement structures (Vol. 1). Washington, DC. ISBN 978-1-56051-055-0. http://habib00ugm.files.wordpress.com/2010/05/aashto1993.pdf

Agentschap Wegen en Verkeer - Vlaamse Overheid. (2019). *Standaardbestek 250 voor de wegenbouw* (versie 4.1). Brussel: Agentschap Wegen en Verkeer – Vlaamse Overheid.

Chen, M.-M., Dere, Y., Sotelino, E. D., & Archer, G. C. (2002). *Mid-panel cracking of Portland cement concrete pavements in Indiana*. Purdue University.

Ecoinvent. (2013). *Lean concrete production, with cement CEM II/A, UPR, ecoinvent 3.6, Undefined*. https://www.globallcadataaccess.org/lean-concrete-production-cement-cem-iia-upr-ecoinvent-36-undefined-0

Engineering Tips. (2004). Density of asphalt concrete. https://www.eng-tips.com/threads/density-of-asphalt-concrete.98308/

Gu, H., Jiang, X., Li, Z., Yao, K., & Qiu, Y. (2019). Comparisons of two typical specialized finite element programs for mechanical analysis of cement concrete pavement.

Lijun, S., & Xinwu, W. (2012). Analysis of load stress for asphalt pavement of lean concrete base. *Physics Procedia, 24* (Part A), 404–411.

Lingannagari, G., Kaloush, K., & Mobasher, B. (2003). *Coefficient of thermal expansion of concrete materials*. Department of Civil and Environmental Engineering, Arizona State University.

Majer, S., Budziński, B., & Lehner, P. (2024). Elastic modulus of cement bound granular material (CBGM). In the *22nd International Conference on Modelling in Mechanics*, Ostrava-Poruba.

Matrix Software. (2023). *Elasticiteitsmodulus voor beton*. https://knowledge-base.matrix-software.com/nl/help/matrix-tools/geotechnics/bending-moment-pile/youngs-modulus-for-concrete

Nawy, E. G. (2008). *Concrete construction engineering handbook* (2nd ed.). CRC Press.

Rens, L. (2020). *Guide for design of jointed plain concrete pavements*. EUPAVE.

Skar, A. (2017). *Deterioration models for cement bound materials in structural design and evaluation of heavy duty pavements* (Doctoral dissertation). Technical University of Denmark.

Seric, L., Korun Curic, K., & Susnjar, M. (2013). Principal component analysis of fatigue strength. In *36th International Convention on Information and Communication Technology, Electronics and Microelectronics, MIPRO 2013 – Proceedings*. Opatija.

Shaban, A. M., Alsabbagh, A., Wtaife, S., & Suksawang, N. (2020). Effect of pavement foundation materials on rigid pavement response. In *IOP Conference Series: Materials Science and Engineering*. Al Khums City.

Swarna, S. T., Gali, R. R. L., Reddy, M. A., & Mehta, Y. (2024). The analysis and design of jointed plain concrete pavements with wider slabs. *Road Materials and Pavement Design, 25*(12), 2664–2684.

EverFE: Software for the 3D finite element analysis of jointed plain concrete pavements. (2025). Civil and Environmental Engineering. https://civil.umaine.edu/everfe-2/

Xu, L. (2016). *Typical values of Young's elastic modulus and Poisson's ratio for pavement materials*.

Yan, C., & Wei, Y. (2023). Dynamic response analysis of JPCP with different roughness levels under moving axle load using a numerical methodology. *Applied Sciences, 13*(19), Article 11046.